

# Automatic Tuning and Matching of a Small Multifrequency Saddle Coil at 4.7 T

Rigoberto Pérez de Alejo,<sup>1\*</sup> Carlos Garrido,<sup>2</sup> Palmira Villa,<sup>1,3</sup> Ignacio Rodriguez,<sup>1</sup> Juan José Vaquero,<sup>4</sup> Jesús Ruiz-Cabello,<sup>1</sup> and Manuel Cortijo<sup>1</sup>

**A new circuit design for automatically tuning and matching a saddle coil for small animal imaging is presented. This design allows working at <sup>1</sup>H, <sup>19</sup>F, and <sup>3</sup>He resonance frequencies in a 4.7 T spectrometer. It is based on a balanced circuit with commercial variable capacity diodes controlled by a computer using digital potentiometers. The change between two different frequencies can be accurately performed in a few seconds. System Q is compared, between 140–210 MHz, to the same coil tuned and matched with high Q variable capacitors. Differences lower than 5% were found with a loaded coil. The proposed design has initially been evaluated in <sup>19</sup>F and <sup>1</sup>H NMR images acquired with a five-tube phantom. An application is also shown for the acquisition of <sup>3</sup>He, <sup>19</sup>F, and <sup>1</sup>H lung images in a control rat.**

**Key words:** magnetic resonance imaging; automatic frequency control; saddle coil; multifrequency NMR

One of the most successful techniques developed during the last years is the use of hyperpolarized noble gas <sup>3</sup>He or <sup>129</sup>Xe (1,2). Direct NMR imaging of other gases, such as fluorinated gases (CF<sub>4</sub>, SF<sub>6</sub>, and C<sub>2</sub>F<sub>6</sub>), has been presented as a new means to study different lung diseases with a different and more economical approach (3). In these multinuclear experiments the use of conventional <sup>1</sup>H MRI is mandatory for planning and localizing the region of interest (ROI), or for combination with perfusion imaging (4). Thus, the use of these multifrequency imaging modalities is very commonplace.

On the other hand, one of the essential prerequisites of any successful NMR experiment is correct probe tuning and matching, particularly for certain biological and medical applications in which time is a limiting factor. Furthermore, the tuning and matching usually change during the course of the experiment for many reasons: e.g., vari-

ation of sample conductivity or size (5). Automatic probe tuning and matching has been done using mechanical (6) or electrical systems. One electrical scheme can be developed using variable capacitors controlled by direct current voltage (varicaps) (7–9). These designs eliminate both having to disturb the electromagnetic environment of the coil and having to try to obtain optimum matching and tuning at both frequencies, although the necessity of an external circuit increases the amount of external noise.

In this study, a new design variant is presented based on the use of varicaps with a computer control system to tune and match a saddle coil. An application of <sup>3</sup>He, <sup>19</sup>F, and <sup>1</sup>H lung images using the proposed design in a control rat at 4.7 T is shown.

## MATERIALS AND METHODS

### Coil Design

A saddle coil (10) was used because of its unique and versatile configuration, which allows better access to the animal located inside, provided that an appropriate coil mechanical support is used (Fig. 1, upper panel). Using the appropriate coil resolves the dilemma of providing required animal comfort under forced space limitations resulting from physiological controls such as a temperature probe, mechanical ventilation (with tracheotomy or endotracheal tubes), and indirect subcutaneous pCO<sub>2</sub> and pO<sub>2</sub> measurements or animal catheterization. Because of its characteristically lumped configuration, it is easy to perform automatic tuning.

The coil size was selected based on practical criteria. A normal saddle coil with an angular width of 120° was designed because the RF shield is well removed from the coil and the wire diameter is very small with respect to the coil perimeter. The diameter and length are equal to 5 cm to ensure a good filling factor and adequate SNR. The effective winding length was reduced by connecting the two parts of the coil in parallel.

The current along the winding length was determined by applying the method of moments (11). The magnetic field distribution in vacuum using the Biot-Savart law was calculated considering the currents in each segment. The quality factor was estimated from inductance and resistance calculations by considering a parallel resonance circuit. From this value, the power requirements were calculated to predict the maximum voltage in the capacitors (12).

### Tuned Circuit

Figure 1 (lower panel) shows the diagram of the tuned circuit. A balanced sample coil was used because a great

<sup>1</sup>Instituto de Estudios Biofuncionales, Universidad Complutense de Madrid, Madrid 28040, Spain.

<sup>2</sup>Instituto de Física de São Carlos, USP, São Carlos, SP 13560-970, Brazil.

<sup>3</sup>Centro de Asistencia a la Investigación de RMN, Universidad Complutense de Madrid, Madrid 28040, Spain.

<sup>4</sup>Unidad de Medicina y Cirugía Experimental, Hospital GU Gregorio Marañón, Madrid 28007, Spain.

Grant sponsor: Spanish Comisión Interministerial de Ciencia y Tecnología (CICYT); Grant number: AGL2001-3792-C02-01 (to R.P.A.); Grant sponsor: Brazilian Fundação de Amparo à Pesquisa do Estado de São Paulo (FAPESP); Grant number: 00/10704-5 (to C.G.); Grant sponsor: CICYT; Grant numbers: SAF2000-0115; TIC2000-0376-P4; Grant sponsor: EC; Grant number: PHIL, QLG1-2000-01559.

\*Correspondence to: Rigoberto Pérez de Alejo, Instituto de Estudios Biofuncionales, Universidad Complutense de Madrid, Paseo Juan XXIII 1, 28040 Madrid, Spain. E-mail: pdeaf@ieb.ucm.es

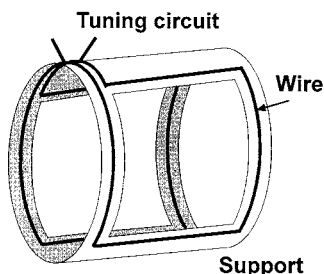
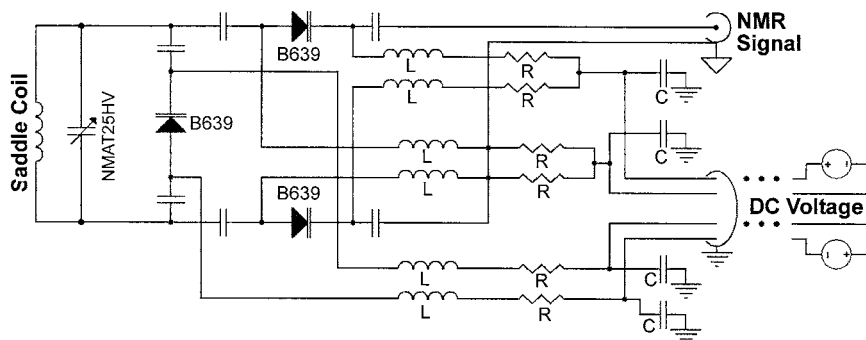


FIG. 1. Diagram of the tuned circuit including a fixed capacitor to increment the Q factor of the resonance circuit.



increase in the NMR SNR appeared (13). The varicaps used were BB639 (Infineon, Munich, Germany), allowing a capacity from 38.3 to 2.4 pf with an applied reverse bias voltage from 1–28V. Fixed capacitors and a variable capacitor from 1–23 pf NMAT25HVFS (Voltronics, Denville, NJ) with a high quality factor (Q) of more than 1500 were fitted to adjust the range of the varicaps to attain the adequate frequency range. This allowed increasing the weighted mean Q of the capacitors.

The varicaps were controlled using a DC voltage through axial RF chokes located in the Faraday shield in order to reduce the RF signal coupling between the varicaps and also to isolate the coil from the DC bias voltage source, avoiding external noise. The matching varicaps (*Dm*) were controlled by applying the same bias voltage to obtain the best balance in the tuned circuit.

#### Automatic Control System

The tuning and matching control was developed in two ways: 1) manual capacity adjustments by the user, and 2) automatically. The voltages are carried to the varicaps through passive low-pass “pi” filters located in the Faraday shield. The voltages were controlled using two potentiometers as a DC (5V) voltage splitter. Finally, a TL082 double operational amplifier (Texas Instruments, Dallas, TX) was used to translate the variable voltage from 0–5V to 0–30V. This scheme is independent of the controller system and assures high stability as well as good isolation. During manual operation single linear and multiturn potentiometers are used, while during automatic operation a double digital potentiometer AD8402 (Analog Devices, Norwood, MA) is used. The external and computer noise (at a frequency higher than 10 MHz) is attenuated by more than 60 db, sufficient to facilitate its elimination during the experiment.

The algorithm used for tuning the system is based on the previous characterization of the tuned coil inside the magnet. However, this may not be sufficient for fine-tuning of the coil because, in practice, several additional parameters affect the circuit tuning: e.g., sample resistance, filling factor, etc. Therefore, a second step was introduced based on a test of all potentiometer positions around the one that resulted from the first process.

#### Coil Evaluation

The system was initially evaluated using a home-made phantom at  $^{19}\text{F}$  and  $^1\text{H}$  frequencies (188.05 and 200.36 MHz at 4.7 T, respectively). It was composed of five small tubes of 1 cm in diameter and 5 cm in length inside a cylindrical enclosure. Three of the tubes and the surrounding space in the enclosure were filled with a solution of  $\text{NiSO}_4$  in water ( $T_1$  from 45–102 ms and  $T_2$  from 36–73 ms) and the other two tubes were filled with  $\text{C}_6\text{F}_6$  solutions in acetone (Proton  $T_1$  from 3400–3900 ms and proton  $T_2$  from 850–1260 ms; fluorine  $T_1$  from 3200–3600 ms and fluorine  $T_2$  from 830–1050 ms).

The same type of high-Q variable capacitors from 1–23 pF were used to analyze the tuned circuit in the classical configuration and to obtain a reference for comparison to the quality of the circuit using varicaps.

First, circuit Q was analyzed in all the frequency ranges allowed by the varicaps, i.e., between 140 and 210 MHz. The theoretical Q was compared to the loaded and unloaded coil, with/without varicaps. This study allows analysis of the frequency possibilities of the system and further possibilities to be used in NMR studies using other nuclei. The Q values were measured using a Hewlett Packard RF Network Analyzer 8712C (HP, Palo Alto, CA).

Afterwards, the SNR was measured using the protocol proposed by the National Electric Manufacturer Associa-

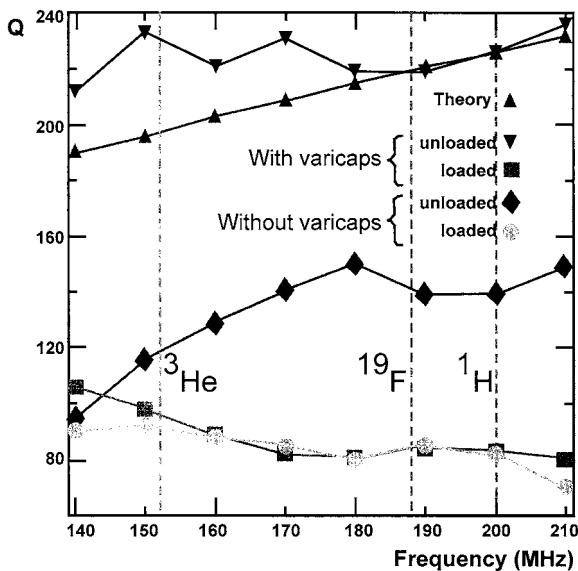


FIG. 2. Plot of the  $Q$  vs. frequency; ( $\square$ ) theoretical result, ( $\circ$ ) and ( $\Delta$ ) results using high  $Q$  variable capacitors unloaded and loaded and crosses ( $\times$ ) and asterisks ( $*$ ) results from the varicaps implementation unloaded and loaded.

tion (NEMA) test (14). All SNR measurements were performed in the slice corresponding to the coil center and in those associated with the two extremes; at 1.5 cm both sides off-center. Images were acquired using a Bruker Biospec 47/40 spectrometer (Ettlingen, Germany) with a standard spin echo sequence:  $128 \times 128$ , field of view (FOV)  $5 \times 5 \text{ cm}^2$ , 2 mm thick slice, TR/TE 1500/12 ms. The SNR at proton and fluorine frequencies, employing high  $Q$  variable capacitors and varicaps, were compared.

Finally, an analysis of the flip angle was completed to evaluate whether the varicaps reach saturation condition. In this case the  $\alpha$ - $2\alpha$  method was used (15). This measurement was only performed using  $^1\text{H}$  MRI because this was sufficient to demonstrate the power behavior of the varicaps in the experiments. We needed to normalize the power scale and to establish the conversion to direct power because Bruker Biospec instruments show the attenuation of the maximum power in db. For this analysis, a new cylindrical phantom of small dimensions (1 cm of diameter and 3 cm of length), doped with  $\text{CuSO}_4$ , was used to minimize the effects of coil nonuniformities.

### In Vivo Application

Images of hyperpolarized  $^3\text{He}$ ,  $^{19}\text{F}$ , and  $^1\text{H}$  in control rat lungs (in the same Bruker NMR spectrometer at 4.7 T) were acquired to evaluate the quality of the system proposed

here. This research complied with European legislation on the care and use of animals, National Institutes of Health (NIH) guidelines for the use of laboratory animals, and related codes of practice.

The rat was anesthetized with sodium pentobarbital (60 mg/Kg, i.p.), tracheotomized, and connected to a low-pressure transducer (Honeywell, Morristown, NJ) to calculate each inspiratory capacity (IC). For MRI experiments, tracheotomy tubes were connected to a customized ventilator and the animal was injected from functional residual capacity with an  $\text{SF}_6$  or hyperpolarized gas volume equivalent to one IC.

For  $^1\text{H}$  MRI, one coronal and one axial slice were acquired using a  $T_1$ -weighted spin echo sequence: TR/TE = 400/15 ms, 4 mm slice thickness,  $256 \times 128$  acquisition points, and FOV  $6 \times 6 \text{ cm}^2$ .

For  $^{19}\text{F}$  imaging, data were acquired during breathhold after filling lungs with fluorinated gas using a radial projection-reconstruction sequence: 5 accumulations, 128 projections of 128 points, FOV  $6 \times 6 \text{ cm}^2$ , TR/TE = 30/0.1 ms to the image time 20 sec (16). In this case, axial and coronal images were also acquired.

$^3\text{He}$  gas was hyperpolarized using depopulation optical pumping of dilute rubidium vapor at 794.8 nm, which then slowly polarizes  $^3\text{He}$  nuclei by spin exchange (17). For  $^3\text{He}$  imaging, data were also acquired during breathhold after filling the lungs with hyperpolarized helium gas using the same radial sequence without accumulations, 128 projections of 128 points, FOV  $6 \times 6 \text{ cm}^2$ , TR/TE = 10/0.1 ms, for a total image time 1.3 sec.

## RESULTS AND DISCUSSIONS

At the proton frequency recorded at 4.7 T, one of the main problems found was that the coil wavelength exceeds  $\lambda/10$  at this frequency. Thus, two unwanted effects appear: radiation losses and different currents along the winding (5). For the dimensions used, the winding length is around 23 cm representing  $\lambda/6.5$  at 200 MHz. On the other hand, the deviation in the currents along the field-generating winding region is  $\sim 9\%$ , a value that is reasonably low for our purposes. Only 26% of the magnetic field mapping in a circular region (4.8 cm) in the axial plane has more than 20% of nonuniformity. The effect of the nonuniform current distribution is very low and is hidden by the magnitude of the nonuniformity, as we can see in the quasisymmetric axial contour.

In the control circuit, digital-to-analog converters have commonly been used (7); here, a new scheme based on digital potentiometers as voltage dividers was used. This option results in high stability and digital noise isolation and facilitates autonomous work after preprogramming

Table 1  
Measures of the SNRs

SNR	$^1\text{H}$ : 200.36MHZ				$^{19}\text{F}$ : 188.50MHZ			
	Slice	Left	Central	Right	Lung	Left	Central	Right
With varicaps		85.4	87.1	86.2	42.4	12.6	13.5	12.8
Without varicaps		92.6	95.8	94.3	39.8	14.8	15.7	15.2

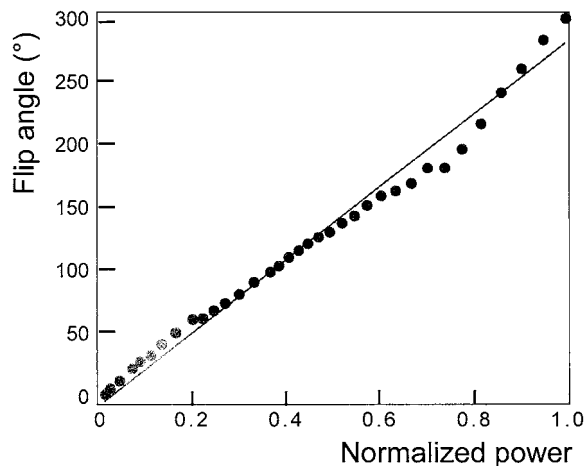


FIG. 3. Plot of the flip angle vs. the normalized power of the NMR instrument. The continuous line represents the lineal response adjustment of these data.

without the need to introduce an expensive, highly isolated operational amplifier.

The Q analysis was included to perform an initial evaluation of the SNR outside the NMR instrument. Figure 2 shows the graphical Q performance as a function of the frequency with and without varicaps and with the coil empty or loaded with a rat. The optimal matching and tuning response of the probe from 140–210 MHz, which includes the frequency of different nuclei at 4.7 T (e.g.,  $^3\text{He}$ , 152.63 MHz,  $^{19}\text{F}$ , 188.53 MHz,  $^1\text{H}$ , 200.36 MHz), increases the flexibility and the range of experimental MRI applications with different nuclei.

The comparison between the theoretical results and the unloaded resonant circuit, using the high Q variable capacitors, is highly consistent with the predicted behavior. The values obtained in all the frequency ranges are higher than 200—excellent for a small diameter coil. After introducing varicaps and the associated circuit (mainly due to the cables and related components used to carry the voltage) the Q values now dropped to lower than 150 in all the frequency ranges. This observed effect, which showed a higher decrease for smaller frequencies, points out the major influence of the inductive elements introduced in the Q. However, in biological samples, and especially in rat lung studies, this is not a problem (whether or not varicaps were used), since the resistance of the sample is the predominant factor in noise generation (18). It is seen in the behavior of the loaded coil, in terms of the Q in both conditions (using both high Q variable capacitors and varicaps), which is very similar in all the frequency ranges used and is always lower than 100. However, at  $^3\text{He}$  frequency, the varicaps version of the coil achieved a  $Q_{\text{unloaded}}/Q_{\text{loaded}} = 1.41$ . Although this indicates relatively low efficiency at this frequency, it is a necessary trade-off for the triple tune feature of the coil. The shift of the frequency did not drop significantly when the coil was loaded both with and without varicaps (1.0%, 0.7%, and 0.5% for  $^1\text{H}$ ,  $^{19}\text{F}$ , and  $^3\text{He}$ , respectively).

From the Q analysis, the expected SNR in biological samples does not appreciably change by using or not using

the proposed scheme based on varicaps. This is seen in the SNR analysis performed in Table 1. The differences between the central and both extreme slices are not significant, meaning that the coil can be satisfactorily employed to study rat lungs and other structures with similar sizes (smaller than 3.4 cm). The SNRs were decreased by  $\sim 9\%$  when the varicaps were introduced. Strictly speaking, this difference can be significantly lower, considering that the tuning and matching is better ensured using an automatic method with respect to one manually performed. Further considerations, such as time savings, are also important.

Figure 3 shows the results obtained in the measurement of the flip angle vs. the normalized power of the NMR machine. In this case it is easily seen that the coil allows a very satisfactory  $90^\circ$  and  $180^\circ$  pulse adjustment.

Figure 4 shows coronal and axial images of the rat lung, using  $^1\text{H}$ ,  $^{19}\text{F}$ , and  $^3\text{He}$ . Fluorine (Fig. 4b) and  $^3\text{He}$  (4c) images were overlaid on proton images (4a). As an example of the possibilities in terms of temporal requirements, these images were consecutively acquired within 4 min. Thus, about  $2 \times 52$  sec were needed to perform a  $^1\text{H}$  single-slice spin echo acquisition,  $2 \times 20$  sec per each  $^{19}\text{F}$  projection reconstruction (axial and coronal),  $2 \times 1.3$  sec per each  $^3\text{He}$  reconstruction projection (also axial and coronal), and less than 2.5 min to change the coil tuning and matching. This last period can be significantly re-

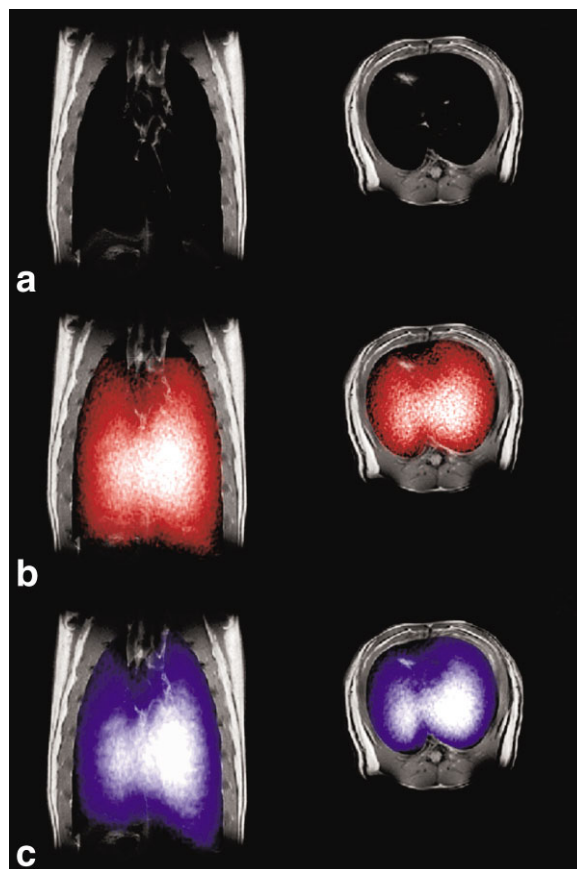


FIG. 4. Coronal (left) and axial (right) images of a control rat lung acquired using the scheme presented in this work: (a) proton images, (b) an overlay of proton and fluorine (red) images, and (c) an overlay of proton and hyperpolarized helium 3 images (blue).

duced, although this has not been attempted yet. This reduction may be mandatory in some special applications and, again, it will increase the number of applications and experimental flexibility.

In our experiments, the design of the saddle coil allows better access for animal control and positioning and provides an extra space for acquisition of physiological parameters. In this case, a pneumatic ventilator was included to control breathing cycles and apnea periods (19).

Previous work has been reported with the same aim. To our best knowledge, the most recent approach to performing multinuclear images was developed for working at 3 T (7) with a coil working at  $^1\text{H}$  and  $^{19}\text{F}$  nuclei frequencies. In our approach, the frequency range was extended to the  $^3\text{He}$  frequency and the system was developed for a 4.7 T magnetic field. In addition to the advantages regarding the higher accessibility referred to in the previous paragraph, the saddle coil is a configuration that minimizes the number of varicaps in the final configuration, avoiding the inclusion of several DC biases to change the capacities and achieving a noise reduction in the system. Finally, the introduction of the balanced circuit enables optimizing the SNR of the coil.

In summary, the main advantages of the system proposed here are time savings and versatility in system operation. In the emerging field of hyperpolarized gases, these two aspects are especially crucial to avoid noble gas depolarization due to short  $T_1$  of storage cells.

## REFERENCES

1. Albert MS, Cates GD, Driehuys B, Happer W, Saam B, Springer CS, Wishnia A. Biological magnetic resonance imaging using laser-polarized  $^{129}\text{Xe}$ . *Nature* 1994;370:199–201.
2. Middleton H, Black RD, Saam B, Cates GD, Cofer GP, Guenther R, Happer W, Hedlung LW, Jonson GA, Juvan K. MR imaging with hyperpolarized  $^3\text{He}$  gas. *Magn Reson Med* 1995;33:271–275.
3. Günther Schreiber W, Eberle B, Laukemper-Ostendorf S, Markstaller K, Weiler N, Scholz A, Bürger K, Heussel CP, Thelen M, Kauczor HU. Dynamic  $^{19}\text{F}$ -MRI of pulmonary ventilation using sulfur hexafluoride ( $\text{SF}_6$ ) gas. *Magn Reson Med* 2001;45:605–613.
4. Cremillieux Y, Berthezene Y, Humblot H, Viallon M, Canet E, Albert T, Heil W, Briguet A. A combined  $^1\text{H}$  Perfusion/ $^3\text{He}$  ventilation NMR in rat lungs. *Magn Reson Med* 1999;41:645–648.
5. Chen CN, Hoult DI. Biomedical magnetic resonance technology. Philadelphia: Medical Science Series, Institute of Physics; 1989. p 117–172.
6. Hwang F, Hoult DI. Automatic probe tuning and matching. *Magn Reson Med* 1998;39 214–222.
7. Muftuler LT, Gulsen G, Sezen KD, Nalcioglu O. Automatic tuned MRI RF coil for multinuclear imaging of small animals at 3T. *J Magn Reson* 2002;155:39–44.
8. Hirata H, Walczak T, Swartz HM. Electronically tunable surface-coil-type resonator for L-band EPR spectroscopy. *J Magn Reson* 2002;142: 159–167.
9. Sugiura S. Automatic tuning circuit for nuclear magnetic resonance apparatus. U.S. Patent 4602213, July 1986.
10. Ginsberg DM, Melchner MJ. Optimum geometry of saddle coils for generating a uniform magnetic field. *Rev Sci Instr* 1970;41:122–123.
11. Harrington RF. Field computation by moment methods. Piscataway, NJ: IEEE Press; 1982.
12. Doty FD, Entzminger G, Hauck JRCD, Staab JP. Practical aspects of birdcage coils. *J Magn Reson* 1999;138:144–154.
13. Murphy-Boesch J, Koretsky AP. An in vivo NMR probe circuit for improved sensitivity. *J Magn Reson* 1983;54:526–532.
14. Sano RM. NEMA Standards: performance standards for clinical magnetic resonance systems. In: Dixon RL, editor. MRI acceptance testing and quality control—the role of the clinical medical physicist. Madison, WI: Medical Publishing; 1988. p 185–189.
15. Perman WH, Bernstein MA, Sandstrom JC. A method for correctly setting the RF flip angle. *Magn Reson Med* 1989;9:16–24.
16. Rodríguez I, Pérez de Alejo R, Cortijo M, Ruiz-Cabello J. COMSPIRA: a common approach to spiral and radial MR imaging. *Concept Magn Reson Imag B* 2004;20:40–44.
17. Walker TG, Happer W. Spin-exchange optical pumping of noble gas pumping. *Rev Mod Phys* 1997;69:629–642.
18. Bottomley PA, Redington RW, Edelstein WA, Schenck JF. Estimating radiofrequency power deposition in body NMR imaging. *Magn Reson Med* 1985;2:336–349.
19. Pérez de Alejo R, Ruiz-Cabello J, Rodríguez I, Villa P, Cortijo M. Respirador versátil multi-modal compatible con RMN. Spain. February 14, 2003. Patent No. 2003–00363.